ADVANCED FUNCTIONAL MATERIALS

Supporting Information

for *Adv. Funct. Mater.,* DOI: 10.1002/adfm.202211257

Mg-Doped $Na_4Fe_3(PO_4)_2(P_2O_7)$/C Composite with Enhanced Intercalation Pseudocapacitance for Ultra-Stable and High-Rate Sodium-Ion Storage

Fangyu Xiong, Jiantao Li, Chunli Zuo, Xiaolin Zhang, Shuangshuang Tan, Yalong Jiang, Qinyou An, Paul K. Chu, and Liqiang Mai**

Supporting Information

Mg-doped $Na_4Fe_3(PO_4)_2(P_2O_7)$/C composite with enhanced intercalation pseudocapacitance for ultra-stable and high-rate sodium-ion storage

Fangyu Xiong, Jiantao Li, Chunli Zuo, Xiaolin Zhang, Shuangshuang Tan, Yalong Jiang, Qinyou An, Paul K. Chu, Liqiang Mai**

Experimental Section

Materials Synthesis

All the reagents using in the synthesis were analytical grade and purchased from the Sinopharm. Firstly, $CH_3COONa·3H_2O$ (4 mmol), $MgSO_4·7H_2O$ (0.15 mmol), $FeSO_4·7H_2O$ (2.85 mmol), $NH_4H_2PO_4$ (4 mmol) and $C_6H_8O_7·H_2O$ (4.5 mmol) were added into deionized water (10 mL). After stirring for 5 min, the solution was dried at 160 °C to obtain precursor. Then, the precursor powders after manually grinding were pre-calcined at 300 °C for 3 h in vacuum with heating rate of 5 °C min^{-1}. The calcined powders were pelletized under 15 MPa pressure disk-shaped mold and calcined at 550 °C for 10 h in vacuum with heating rate of 5 °C min^{-1}. Finally, the pellet was ground to obtain $Na_4Fe_{2.85}Mg_{0.15}(PO_4)_2(P_2O_7)$ powders (denoted as NFPP-Mg5%). In addition, the $Na_4Fe_3(PO_4)_2(P_2O_7)$ and $Na_4Fe_{2.7}Mg_{0.3}(PO_4)_2(P_2O_7)$ samples (denoted as NFPP-0 and NFPP-Mg10%, respectively) were synthesized in the same procedure by regulating the molar ratio of $MgSO_4·7H_2O$ and $FeSO_4·7H_2O$ to 0.0:1.0 and 0.1:1.0, respectively. The bare NFPP and NFPP-0 with lower carbon content (denoted as NFPP-0-LC) were synthesized by reducing the amount of $C_6H_8O_7·H_2O$ to 0 and 2.25 mmol, respectively.

Materials Characterizations

X-ray diffraction (XRD) patterns were collected using a D2 Advance X-ray diffractometer (Bruker) with a Cu Kα X-ray source. Fourier transform infrared (FTIR) spectra were measured by using Nicolet iS50 FTIR spectrometer in diffuse reflectance mode. Raman spectroscopy experiments were performed on the HORIBA LabRAM HR Evolution micro-Raman spectroscopy system with the 523 nm laser. X-ray photoelectron spectroscopy (XPS) measurements were carried out using Kratos Axis Supra XPS instrument. Field-emission scanning electron microscopy (FESEM) images were obtained by using JEOL-7100F microscope. Transmission electron microscopy (TEM) and high-resolution TEM (HRTEM)

images, selected area electron diffraction (SAED) pattern, high-angle ring dark field image-scanning transmission electron microscope (HAADF-STEM) images, and energy dispersive spectroscopy (EDS) elemental mappings were recorded by using a Titan G2 60-300 microscope. The TG analysis was conducted on a STA 449F3 thermoanalyzer under an air atmosphere from 30 to 600 °C with a heating rate of 10 °C min^{-1}.

Electrochemical Measurement

CR2016 coin cells were assembled in an Ar-filled glove box with sodium metal foil as the anode, glass fiber membrane (GF/A What-man) as the separator and 1 M $NaPF_6$ dissolved in propylene carbonate (PC) with 5% fluoroethylene carbonate (FEC) as the electrolyte. The cathodes were prepared by spreading the mixed slurry composed of 70 wt% as-synthesized materials, 20 wt% acetylene black, and 10 wt% polyvinylidene fluoride (PVDF) to Al foils and dried at 70 °C. The mass loading of the active material is about 1.5 mg cm^{-2}. Hard carbon anode were prepared by spreading the mixed slurry composed of 70 wt% hard carbon (purchased from Guangdong Canrd New Energy Technology Co., Ltd.), 20 wt% acetylene black, and 10 wt% polyvinylidene fluoride (PVDF) to Al foils and dried at 70 °C. For full sodium-ion batteries, 1 M $NaPF_6$ dissolved in PC with 5% FEC or 1 M $NaPF_6$ dissolved in diethylene glycol dimethyl ether (DEGDME) was used as electrolyte, and both cathode and anode were pre-cycled for 3 cycles before assembling. Galvanostatic charge/discharge and galvanostatic intermittent titration technique (GITT) tests were performed by using a multi-channel battery test system (LAND CT2001A). The GITT curves were obtained at the constant current pulse of 50 mA g^{-1} with the pulse time of 10 min and followed by a relaxation period of 30 min. Cyclic voltammetry (CV) curves and electrochemical impedance spectroscopy (EIS) plots were tested using a BioLogic VMP3 multichannel electrochemical workstation. The multi-scan CV curves were tested on IviumStat multichannel electrochemical workstation. For I-V measurement, the samples were pelletized under 15 MPa pressure disk-shaped mold, and then the pelletized disc was sandwiched between two stainless steel electrodes. The I-V plots were collected using a BioLogic VMP3 multichannel electrochemical workstation.

Table S1. Rietveld refinement data of NFPP-0 and NFPP-Mg5%

Samples	NFPP-0	NFPP-Mg5%
Crystal system	Orthorhombic	Orthorhombic
Space group	Pn21a (No. 33)	Pn21a (No. 33)
Lattice parameter *a*	17.9346(2) Å	17.8919(2) Å
Lattice parameter *b*	6.5395(5) Å	6.5371(8) Å
Lattice parameter *c*	10.7090(1) Å	10.6819(3) Å
Unit-cell volume	1255.99(8) $Å^3$	1249.38(7) $Å^3$

Table S2. Electrochemical performance comparison of NFPP-Mg5% and other reported NFPP-based cathode materials for SIBs

Materials	Rate performance Capacity (mAh g^{-1})/current density (mA g^{-1})	Cycling performance Capacity retention/cycle number/current density (mA g^{-1})	Ref.
NFPP/C nanoparticles	99/25.8, 97/64.5, 95/129, 92/258, 86/645, 78/1,290	89%/300/64.5	[S1]
NFPP/C embedded in graphene	107/64.5, 99/129, 95/258, 88/645, 85/1,290, 78/2,580, 66/6,450	83%/300/2,580	[S2]
NFPP/C nanoparticles	~105/12.9, ~100/25.8, ~80/64.5, ~62/129, ~30/258, ~10/387, ~5/645, ~5/1,290	79%/50/64.5	[S3]
3D graphene decorated NFPP microspheres#	117.4/12.9, 111.9/25.8, 107.3/64.5, 104.5/129, 102.7/258, 96.3/645, 92.6/1,290, 85.3/2,580, 69.7/6,450, 55/12,900, 32.1/25,800	62.3%/6,000/1,290	[S4]
NFPP@$NaFePO_4$@C on carbon cloth	127/64.5, 118/129, 113/258, 104/645, 97/1,290, 89/2,580, 75/6,450, 68/12,900	>100%/3,000/1290 ~90%/3,000/6450	[S5]
NFPP/C nanospheres#	108.2/25.8,105.2/64.5, 102.4/129, 101.2/258, 99.6/645, 97.4/1,290, 95.5/2,580, 92.3/3,870, 90.4/6,450, 77.9/10,320, 67.7/12,900	63.5%/4,000/1290	[S6]
Nanoplate-like NFPP/C	113.0/6, 108.3/12, ~105/24, ~102/60, ~100/120, ~95/360, ~89/600, ~84/1,200, 80.3/2,400	69.1%/4,400/2,400	[S7]
Nanospherical NFPP on MCNTs	115.7/12.9, 107.7/25.8, 103.3/64.5, 99.2/129, 96.7/258, 94/387, 90.5/645, 86.6/1,032, 82.1/1,290, 72.6/1,935, 62.8/2,580	96%/1,200/258	[S8]
Hollow-sphere-structured NFPP/C	107.7/25.8, 103.1/64.5, 101.2/129, 98.6/258, 94.4/645, 85.5/1,290, 72.9/2,580, 64.4/3,870	92%/1,500/1290	[S9]
Ultra-small NFPP particles embedded	106.4/12.9, ~100/25.8, ~96/64.5 89.0/129, ~82/258, ~68/645,	72%/5,000/6,450	[S10]

in carbon nanoribbons[#]	~62/1,290, 57.6/2,580, 46.3/6,450, 30.7/12,900		
Fe-deficient NFPP/C composite	~113/12.9, ~111/25.8, ~107/64.5, ~104/129, ~101/258, ~97/645, ~93/1,290, ~87/2,580, ~70/6,450, ~52/12,900	~95%/10,000/1,290	[S11]
Mn-doped NFPP/rGO composite	107.1/129, 103.3/258, 97.3/645, 90.8/1,290, 83.1/2,580, 77.6/3,870, 69.6/6,450	97.2%/2,000/1,290	[S12]
NFPP-Mg5%	104/50, 100/100, 96/200, 92/500, 89/1,000, 84/2,000, 76/5,000, 66/10,000, 40/20,000	80.8%/14,000/5,000	This work

[#]The capacity in original literature is based on the mass of NFPP, and the capacity in here is based on the total mass of composite.

Table S3. The specific values of the parameters used for the calculation of Na-ion diffusivites from GITT results.

Samples	m_B	V_M	M_B	S
NFPP-0	1.057 mg	189.21 $cm^3\ mol^{-1}$	623.38 $g\ mol^{-1}$	0.785 cm^2
NFPP-Mg5%	1.323 mg	189.21 $cm^3\ mol^{-1}$	623.38 $g\ mol^{-1}$	0.785 cm^2
NFPP-Mg10%	1.428 mg	189.21 $cm^3\ mol^{-1}$	623.38 $g\ mol^{-1}$	0.785 cm^2

Table S4. Equivalent circuit fitting parameters of EIS plots

Elements	NFPP-0	NFPP-Mg5%	NFPP-Mg10%
R_0 (Ohm)	2.4	2.2	2.1
R_1 (Ohm)	57.1	67.3	52.9
R_2 (Ohm)	123.1	92.2	106.7
R_{Ma} (Ohm)	220.6	102.2	141.6

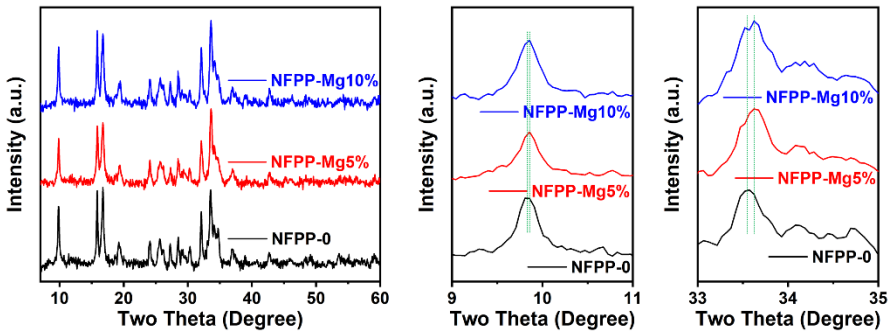

Figure S1. XRD patterns of XRD patterns of NFPP-0, NFPP-Mg5% and NFPP-Mg10%

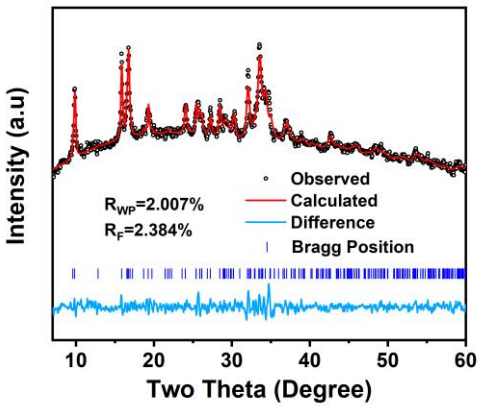

Figure S2. Rietveld refinement of XRD pattern of NFPP-0

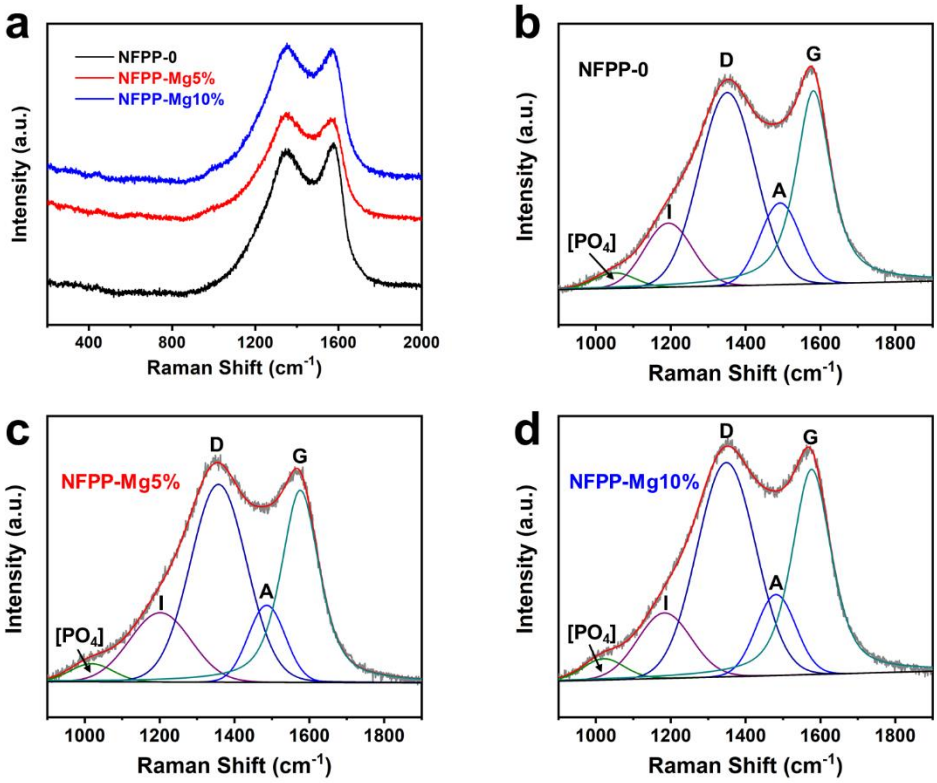

Figure S3. (a) Raman spectra of NFPP-0, NFPP-Mg5% and NFPP-Mg10%, and fitted Raman spectra of (b) NFPP-0, (c) NFPP-Mg5% and (d) NFPP-Mg10%.

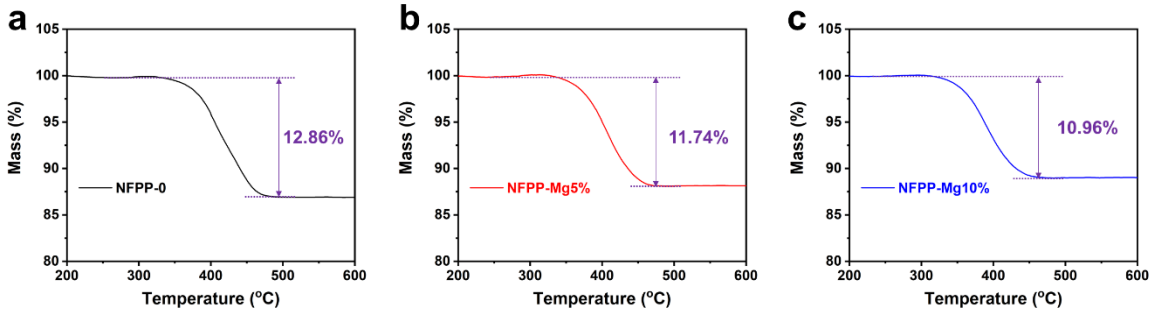

Figure S4. TG curves of (a) NFPP-0, (b) NFPP-Mg5% and (c) NFPP-Mg10% at 10 °C min^{-1} in air atmosphere

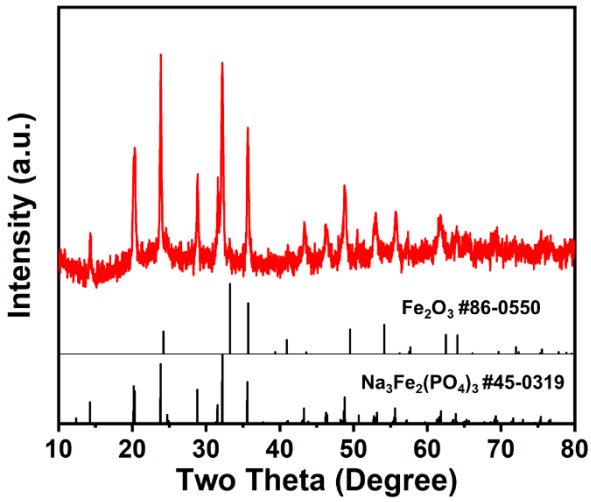

Figure S5. XRD pattern of NFPP-0 after annealing at 600 ºC in air for 2 h

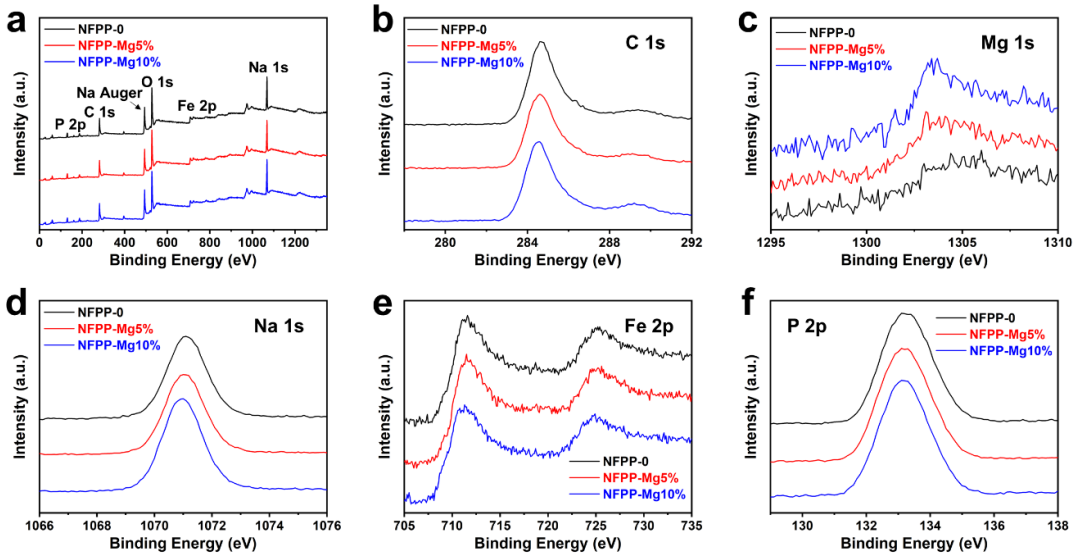

Figure S6. (a) Survey, (b) C 1s, (c) Mg 1s, (d) Na 1s, (e) Fe 2p and (f) P 2p XPS spectra ofNFPP-0, NFPP-Mg5% and NFPP-Mg10%

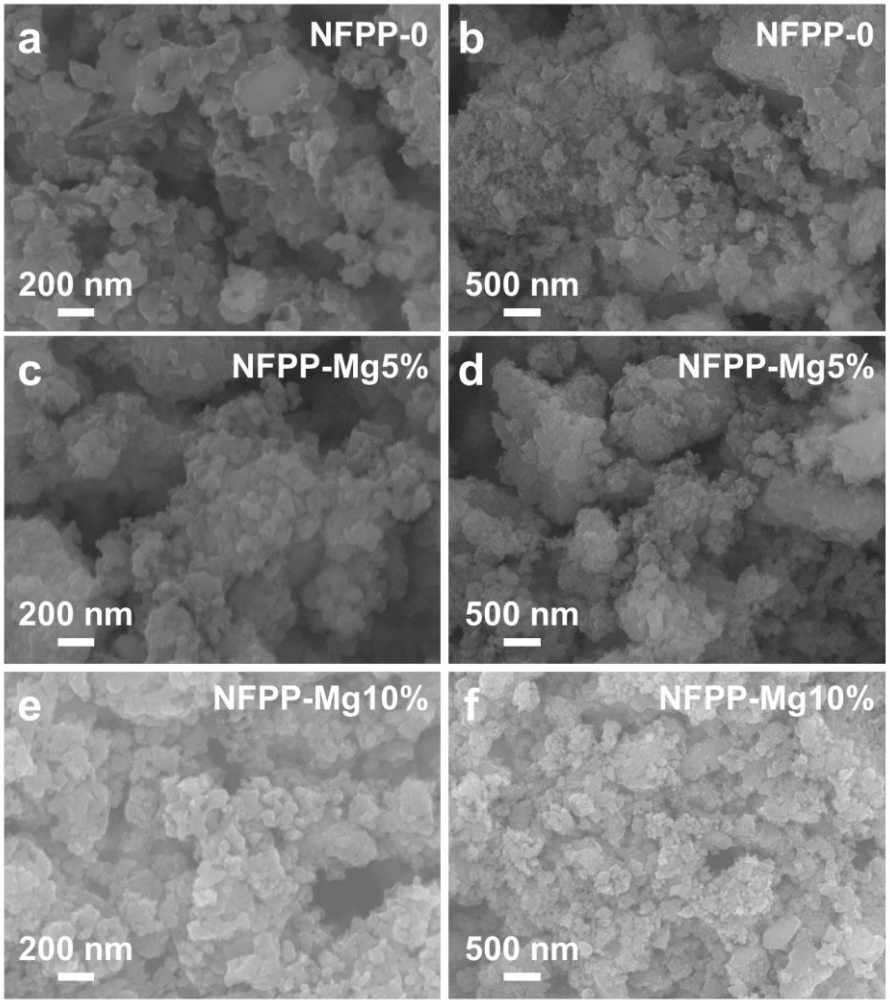

Figure S7. SEM images of (a, b) NFPP-0, (c, d) NFPP-Mg5% and (e, f) NFPP-Mg10%

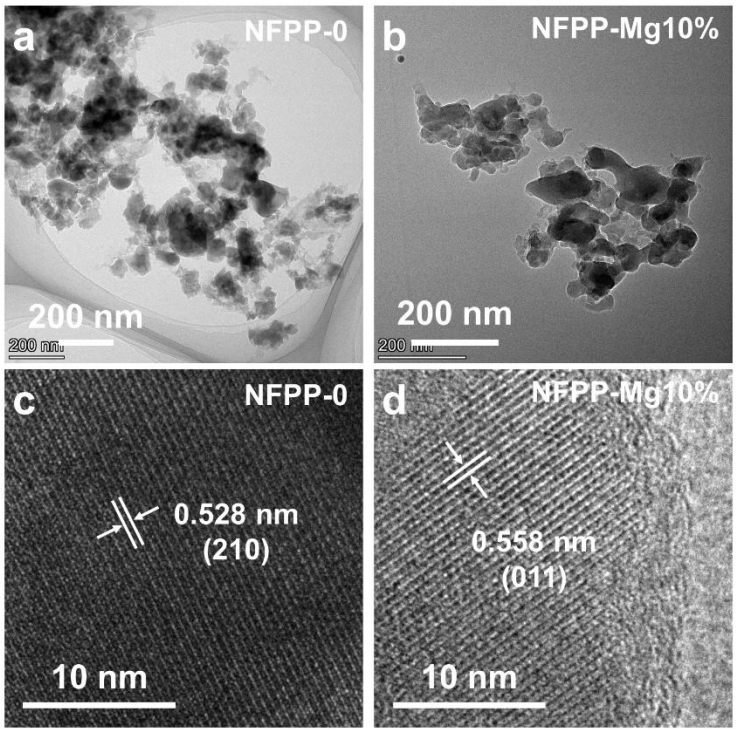

Figure S8. TEM images of (a) NFPP-0 and (b) NFPP-Mg10%, and HRTEM images of (c) NFPP-0 and (d) NFPP-Mg10%

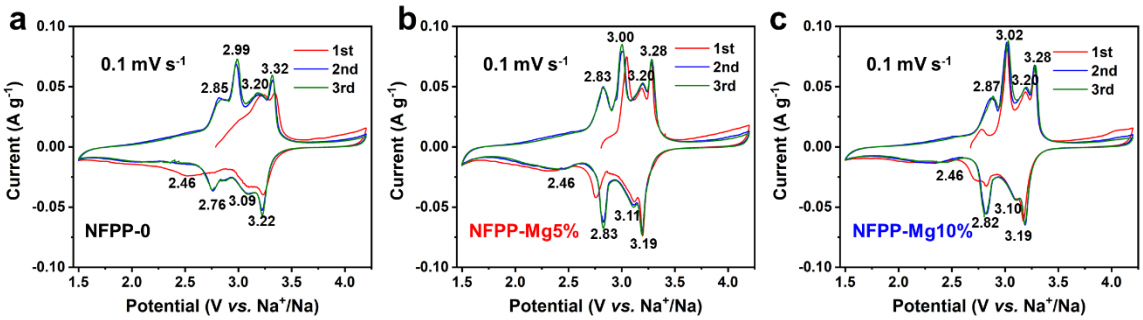

Figure S9. CV curves of (a) NFPP-0, (b) NFPP-Mg5% and (c) NFPP-Mg10% at 0.1 mV s^{-1}

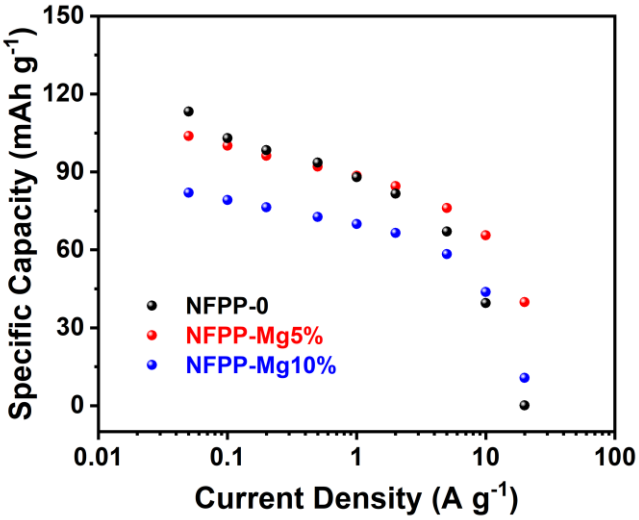

Figure S10. Modified Peukert plots of NFPP-0, NFPP-Mg5% and NFPP-Mg10%

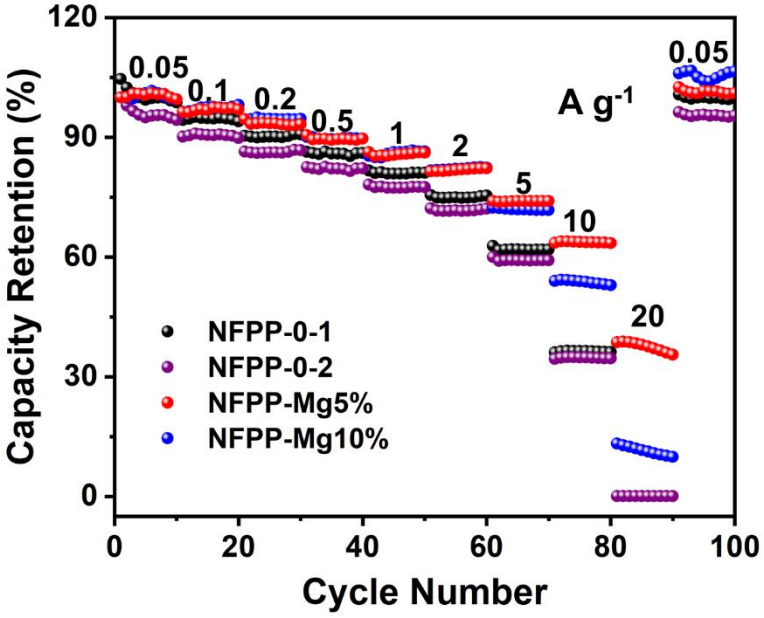

Figure S11. Capacity retentions of NFPP-0, NFPP-Mg5% and NFPP-Mg10% during rate performance test. For NFPP-0-1, NFPP-Mg5% and NFPP-Mg10%, capacity retentions were calculated based on initial capacity, and for NFPP-0-2, capacity retentions were calculated based on the capacity in the fourth cycle.

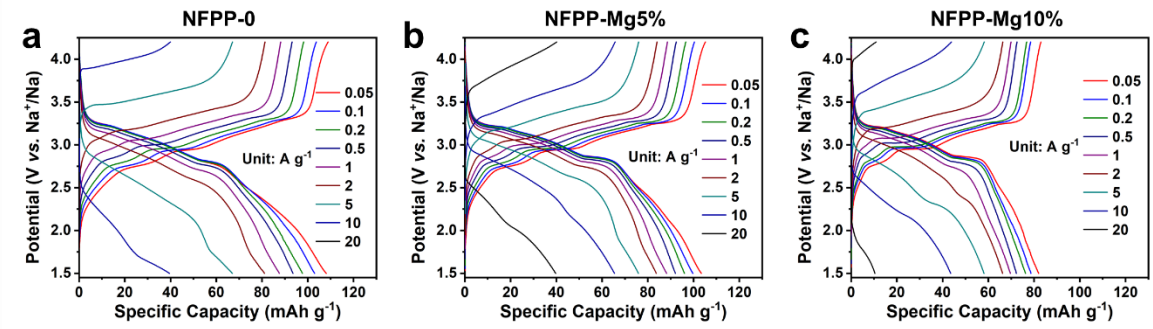

Figure S12. Charge/discharge curves of (a) NFPP-0, (b) NFPP-Mg5% and (c) NFPP-Mg10% at different current densities

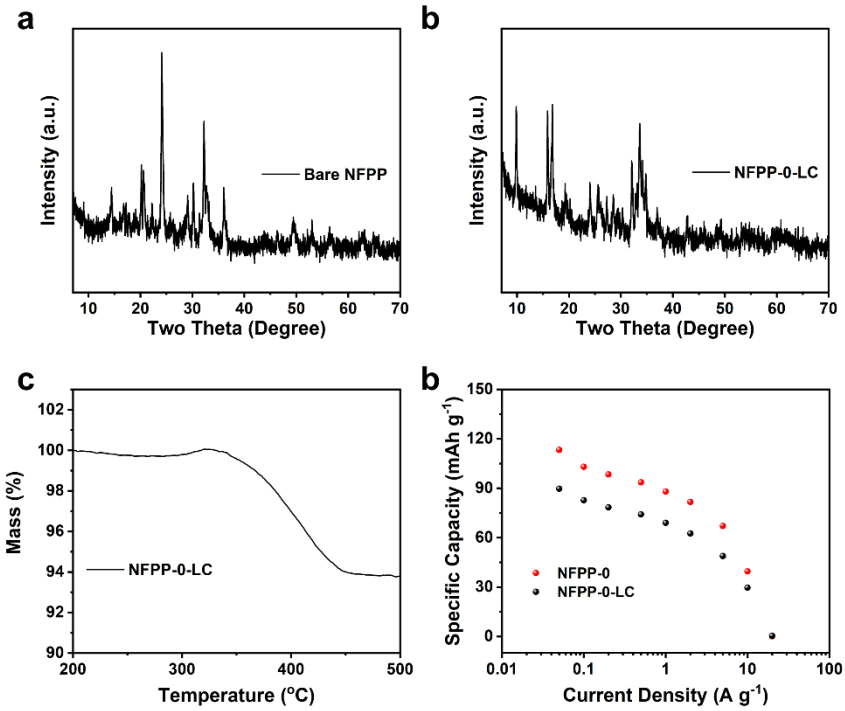

Figure S13. XRD patterns of (a) bare NFPP and (b) NFPP-0-LC, (c) TG curves of NFPP-0-LC in air, (d) modified Peukert plots of NFPP-0 and NFPP-0-LC

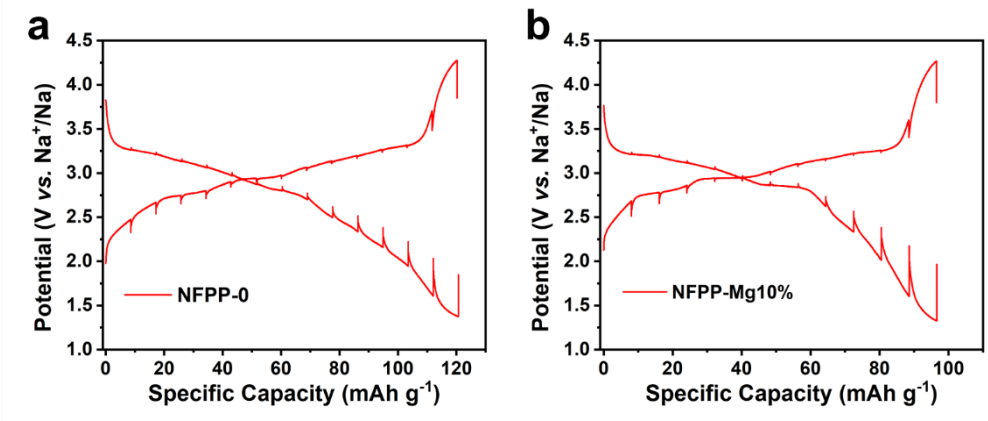

Figure S14. GITT curves of (a) NFPP-0 and (b) NFPP-Mg10% at different current densities

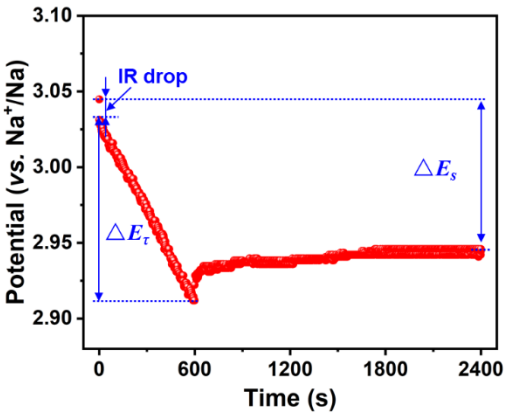

Figure S15. Potential-time curves of NFPP-5% in one current pulse period during the GITT test

The calculation of sodium-ion diffusivities from GITT curves was based on the following equation:

$$D^{GITT} = \frac{4}{\pi\tau}\left(\frac{m_B V_M}{M_B S}\right)^2 \left(\frac{\triangle E_S}{\triangle E_\tau}\right)^2$$

Where τ refers to constant current pulse time, m_B, V_M, M_B, and S are the mass, molar volume, molar mass, and electrode-electrolyte interface area, respectively. $\triangle E_S$ is the voltage difference of one pulse-relaxation period, and $\triangle E_\tau$ is the voltage difference of one constant current pulse (**Figure S15**).

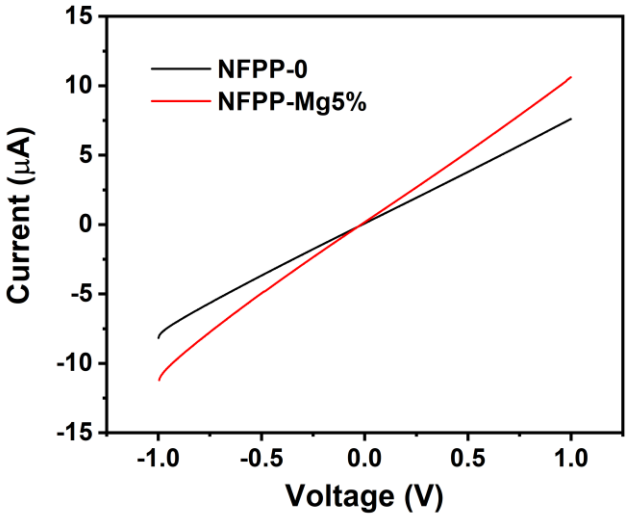

Figure S16. I-V plots of NFPP-0 and NFPP-Mg5%

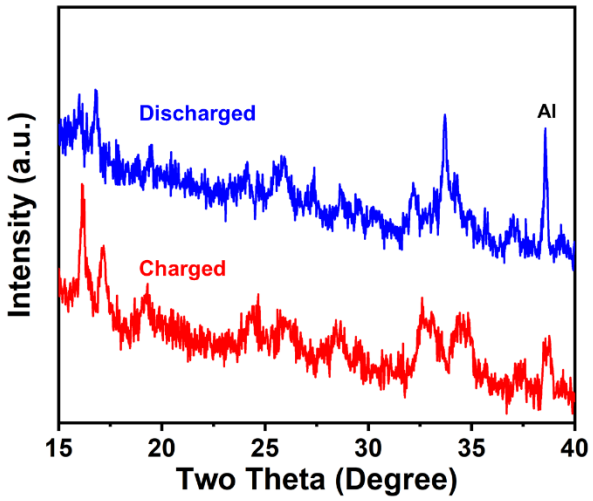

Figure S17. XRD patterns of charged and discharged NFPP-Mg5%

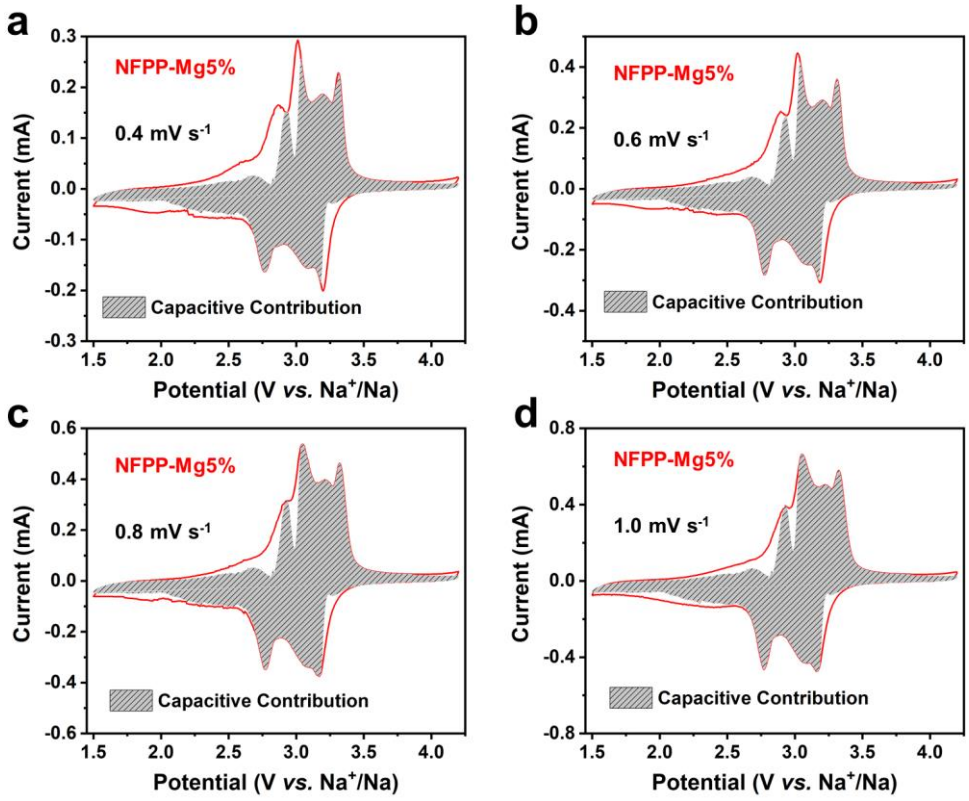

Figure S18. CV curves of NFPP-Mg5% at (a) 0.4, (b) 0.6, (c) 0.8, and (d) 1.0 mV s^{-1} with the calculated capacitive current contribution shown by the gray shaded region

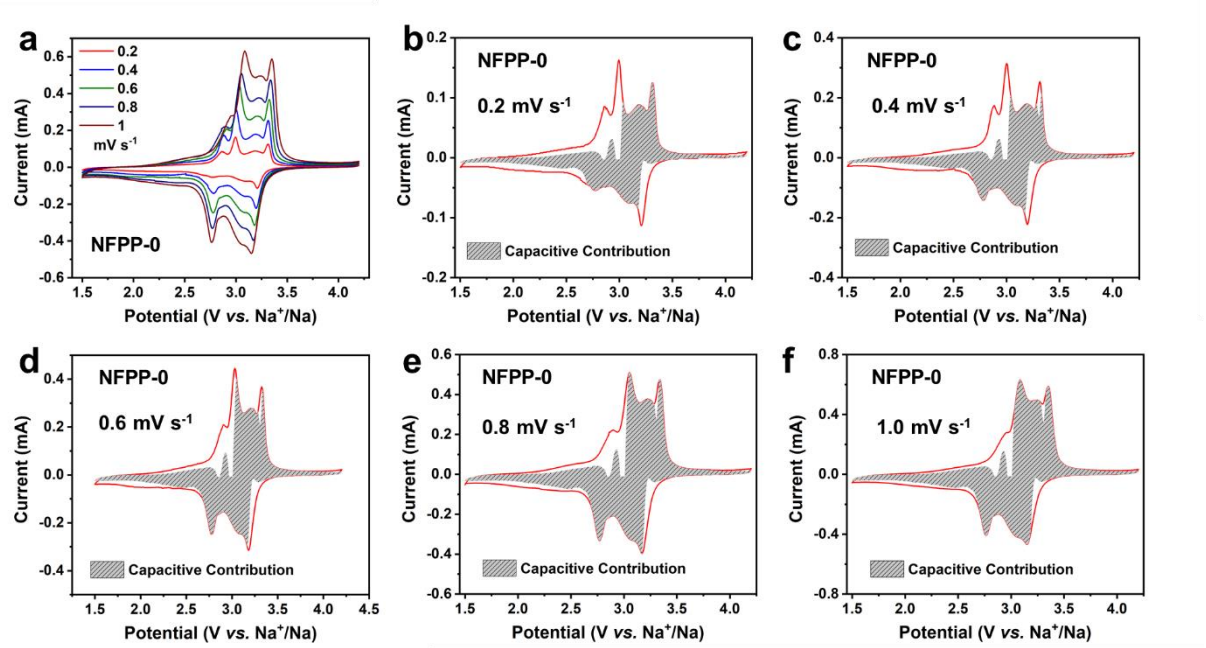

Figure S19. (a) CV curves of NFPP-0 at different scan rates, and CV curves of NFPP-0 at (b) 0.2, (c) 0.4, (d) 0.6, (e) 0.8 and (f) 1 mV s^{-1} with the calculated capacitive current contribution shown by the gray shaded region.

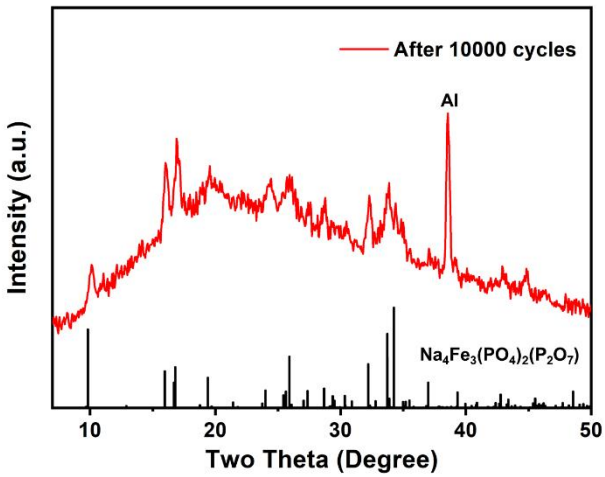

Figure S20. XRD pattern of NFPP-Mg5% after 10,000 cycles at 5 A g^{-1}

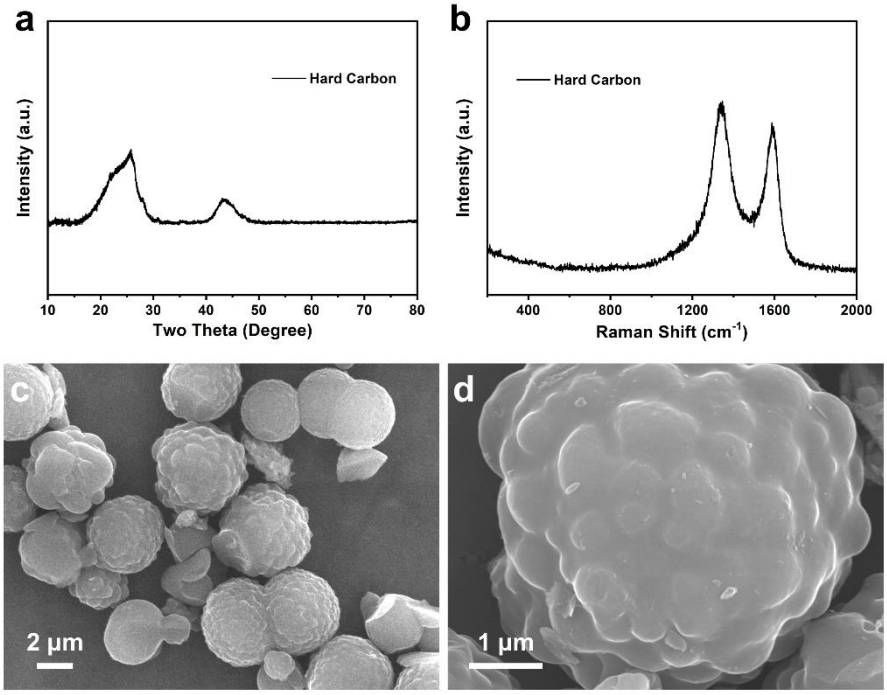

Figure S21. (a) XRD pattern, (b) Raman spectrum and (c, d) SEM images of hard carbon

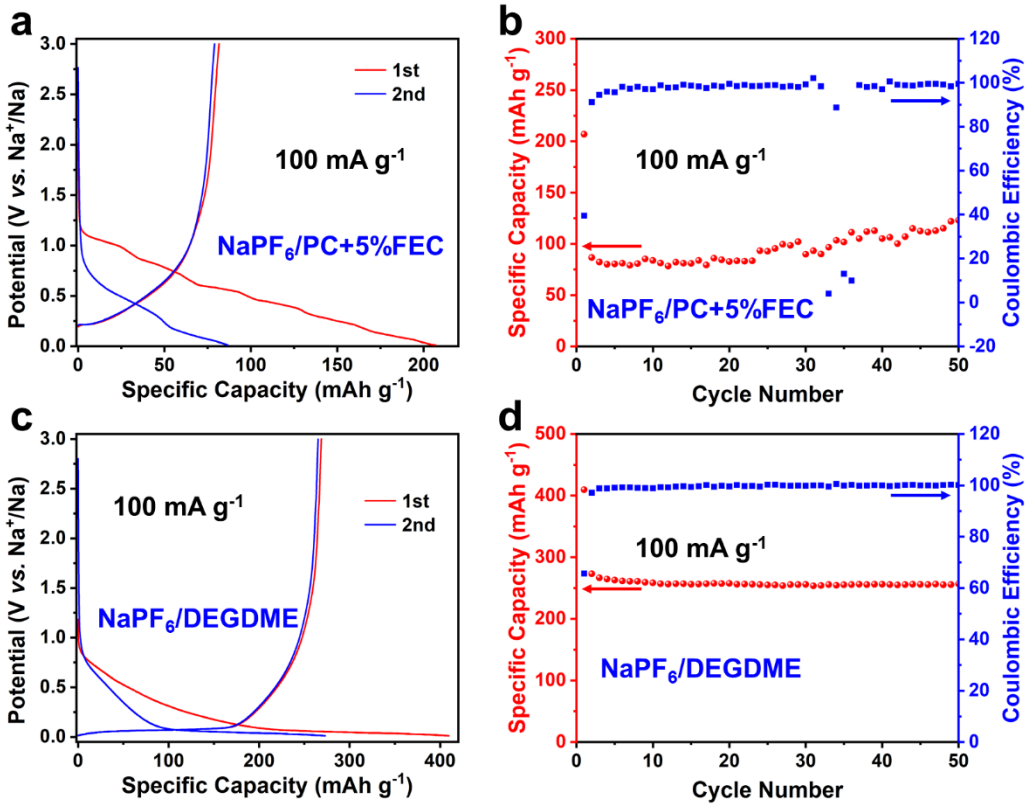

Figure S22. (a, c) Charge/discharge curves and (b, d) cycling performance of hard carbon anode in (a, b) 1 M $NaPF_6$/PC+5%FEC and (c, d) 1 M $NaPF_6$/DEGDME electrolytes

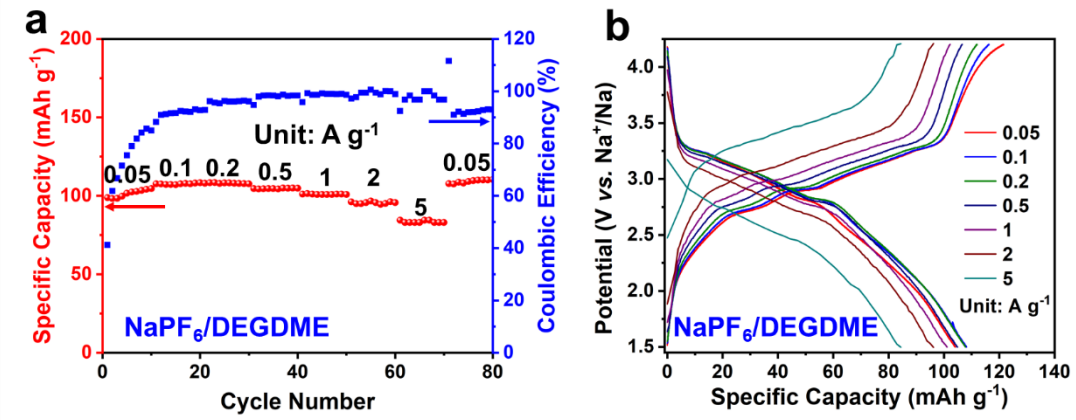

Figure S23. (a) Rate performance and (b) corresponding charge/discharge curves at different current densities of NFPP-Mg5% using 1 M $NaPF_6$/DEGDME electrolyte

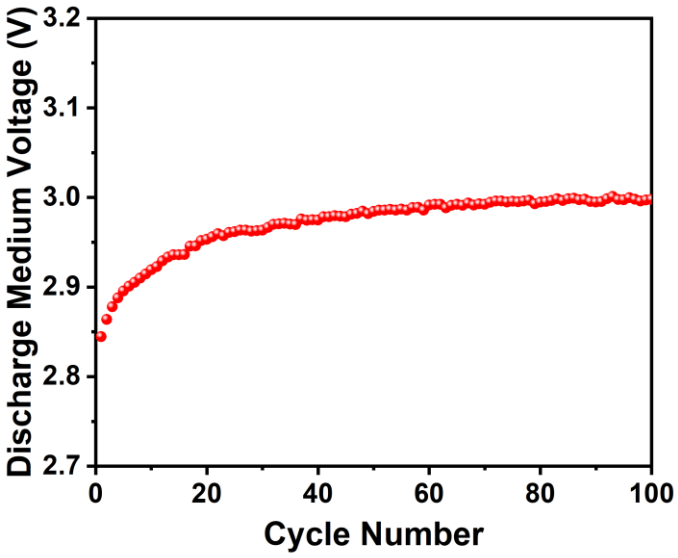

Figure S24. The discharge medium voltage at different cycles of full SIB using $NaPF_6$/DEGDME electrolyte at 500 mA g^{-1}

References

[S1] X. Wu, G. Zhong, Y. Yang, *J. Power Sources* **2016**, *327*, 666.

[S2] X. Ma, X. Wu, P. Shen, *ACS Appl. Energy Mater.* **2018**, *1*, 6268.

[S3] N. V. Kosova, V. A. Belotserkovsky, *Electrochim. Acta* **2018**, *278*, 182.

[S4] T. Yuan, Y. Wang, J. Zhang, X. Pu, X. Ai, Z. Chen, H. Yang, Y. Cao, *Nano Energy* **2019**, *56*, 160.

[S5] X. Ma, Z. Pan, X. Wu, P. K. Shen, *Chem. Eng. J.* **2019**, *365*, 132.

[S6] X. Pu, H. Wang, T. Yuan, S. Cao, S. Liu, L. Xu, H. Yang, X. Ai, Z. Chen, Y. Cao, *Energy Storage Mater.* **2019**, *22*, 330.

[S7] M. Chen, W. Hua, J. Xiao, D. Cortie, W. Chen, E. Wang, Z. Hu, Q. Gu, X. Wang, S. Indris, S. L. Chou, S. X. Dou, *Nat. Commun.* **2019**, *10*, 1480.

[S8] Y. Cao, X. Xia, Y. Liu, N. Wang, J. Zhang, D. Zhao, Y. Xia, *J. Power Sources* **2020**, *461*, 228130.

[S9] L. M. Zhang, X. D. He, S. Wang, N. Q. Ren, J. R. Wang, J. M. Dong, F. Chen, Y. X. Li, Z. Y. Wen, C. H. Chen, *ACS Appl. Mater. Interfaces* **2021**, *13*, 25972.

[S10] J. Zhang, L. Tang, Y. Zhang, X. Li, Q. Xu, H. Liu, Z.-F. Ma, *J. Power Sources* **2021**, *498*, 229907.

[S11] A. Zhao, T. Yuan, P. Li, C. Liu, H. Cong, X. Pu, Z. Chen, X. Ai, H. Yang, Y. Cao, *Nano Energy* **2022**, *91*, 106680.

[S12] X. Li, Y. Zhang, B. Zhang, K. Qin, H. Liu, Z.-F. Ma, *J. Power Sources* **2022**, *521*, 230922.